

Liquid crystal phases of dipolar discotic particles

G. Ayton,¹ D. Q. Wei,² and G. N. Patey¹

¹*Department of Chemistry, University of British Columbia, Vancouver, British Columbia, Canada V6T 1Z1*

²*Centre de Recherche en Calcul Appliqué, 5160 boulevard Decarie, Bureau 400, Montreal, Quebec, Canada H3X 2H9*

(Received 26 July 1996)

Fluids of dipolar oblate ellipsoids of revolution are investigated in detail employing molecular dynamics simulations. For aspect ratios (height-to-breadth) between ~ 1.2 and ~ 3 , it is shown that these systems may form two liquid crystal phases. These are a ferroelectric phase which is stable at higher temperatures and an antiferroelectric columnar phase which is stable at lower temperatures. A partial phase diagram is given and the important structural features of these phases are determined and discussed. [S1063-651X(96)12412-0]

PACS number(s): 64.70.Md, 77.80.-e, 82.20.Wt

I. INTRODUCTION

It is known both from experiment [1,2] and computer simulations [3–6] that disk-shaped or discotic particles form liquid crystal phases. In particular, nematic and columnar phases have been observed. The nematic director, $\hat{\mathbf{d}}$, is associated with the alignment of the symmetry axes of the particles. In the columnar phase the particles are arranged in columns creating long-range spatial order.

Fluids of discotic particles with a point dipole embedded along the symmetry axis have also been investigated with computer simulations [7,8]. In these simulations the particles were modeled as cut spheres with length L and diameter D chosen such that $D/L=10$. Two columnar phases were observed. At low dipole moments unpolarized columns were found. At higher dipole moments, completely polarized columns were observed but equal numbers were polarized in opposite directions such that the total polarization of the system was zero. The columns were arranged with hexagonal symmetry but the “up” and “down” columns were not arranged in any well defined manner. No ferroelectric phases were observed for this model. This behavior is consistent with that of fluids of dipolar prolate ellipsoids [9] and spherocylinders [7,10] which also do not form any ferroelectric liquid phase. However, it contrasts with that of strongly interacting dipolar spheres which have a well defined ferroelectric nematic phase [11,12].

It is evident that particle shape has a significant role in determining the stability of ferroelectric liquid phases. However, the influence of particle shape has not been systematically investigated and understood. The present paper is a step in that direction. We use molecular dynamics (MD) simulations to investigate the phase behavior of fluids of dipolar oblate ellipsoids of varying aspect ratio. A partial phase diagram is presented and discussed. It is shown that interesting ferroelectric behavior exists at intermediate aspect ratios.

II. MODEL AND SIMULATION DETAILS

We consider oblate ellipsoids of revolution with point dipoles embedded at the center as shown in Fig. 1 (note that $\sigma_1 = \sigma_2$ in the present application). The pair potential is of the form

$$u(12) = u_{\text{rep}}(12) + u_{\text{DD}}(12), \quad (1)$$

where $u_{\text{rep}}(12)$ represents a repulsive (rep) Gaussian ellipsoid interaction and

$$u_{\text{DD}}(12) = -3(\boldsymbol{\mu}_1 \cdot \mathbf{r})(\boldsymbol{\mu}_2 \cdot \mathbf{r})/r^5 + \boldsymbol{\mu}_1 \cdot \boldsymbol{\mu}_2/r^3 \quad (2)$$

is the dipole-dipole (DD) potential. In Eq. (2), $\boldsymbol{\mu}_i$ is the dipole associated with particle i , $\mathbf{r} = \mathbf{r}_2 - \mathbf{r}_1$, and $r = |\mathbf{r}|$. The Gaussian ellipsoid interaction or Gaussian overlap potential was introduced by Berne and Pechukas [13] for ellipsoids of revolution and we have since extended the method to the general case [14]. In the notation of [14], $u_{\text{rep}}(12)$ can be expressed in the general form

$$u_{\text{rep}}(12) = 4\epsilon' \exp\left[s\left(1 - \frac{r^2}{\sigma'^2}\right)\right], \quad (3a)$$

where

$$\epsilon' = \epsilon \frac{\sqrt{|\mathbf{b}_1 + \mathbf{b}_2|}}{\sqrt{|\mathbf{T}_1 + \mathbf{T}_2|}}, \quad (3b)$$

$$\frac{r^2}{\sigma'^2} = -(\mathbf{B}\mathbf{B}/4A - \mathbf{C}) : \mathbf{r}\mathbf{r} \quad (3c)$$

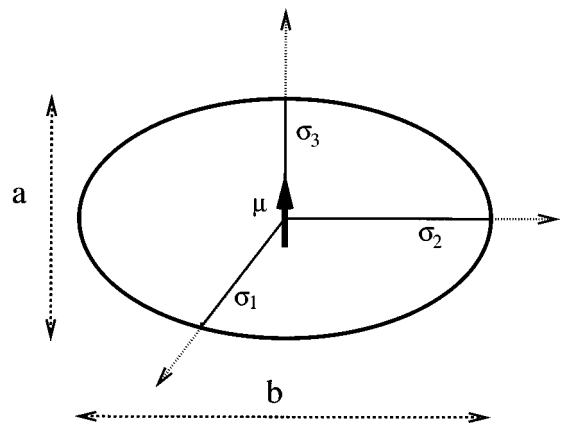


FIG. 1. A sketch of the dipolar ellipsoid model. All relevant labels are explained in the text.

and explicit expressions for the matrices \mathbf{b} , \mathbf{T} , \mathbf{C} , as well as the vector \mathbf{B} and the scalar A are given in the appendix. In Eq. (3a), s can be regarded as a ‘‘hardness’’ parameter which determines the strength and range of the repulsive potential. As s becomes larger the potential becomes sharper and the particles behave essentially as hard ellipsoids. In this case, σ' is approximately the distance of closest approach for two particles at their respective orientations. In the present calculations $s=20$ was used. This gives a very sharp and rapidly decaying potential. Calculations with larger values of s gave very similar results.

The properties of the system were explored by carrying out constant temperature MD simulations [15] employing periodic boundary conditions and the Ewald summation method [16]. Most calculations were carried out with 256 particles but some runs with $N=500$ were done to ensure that the results obtained were not significantly dependent on system size. The dielectric constant of the surrounding continuum [16] ϵ' was taken to be ∞ in most simulations. Tests with $\epsilon'=1$ gave similar results in isotropic systems and the expected domain structure was observed in ferroelectric phases [11]. All simulations were carried out using the reduced time step, $\delta t^* = \delta t \sqrt{ma^2/\epsilon} = 0.0012$ (m is the mass, $a \equiv 2\sigma_3$ is the particle ‘‘height’’). All simulations were initiated with oblate particles on a face-centered-cubic lattice. The system was then equilibrated for 20 000 time steps with no dipolar interactions at the density and temperature of interest. A configuration was then chosen from the equilibrated isotropic system (note that without dipolar forces all systems considered here would be isotropic) and the dipolar forces were switched on. Equilibration runs of 100 000 time steps were then followed with production runs of 200 000 time steps over which the averages of interest were taken. Standard deviations were estimated by dividing the production runs into ten equal blocks and assuming that the block averages were independent measurements.

We are mainly interested in orientational order and this was detected by calculating the first- and second-rank order parameters, $\langle P_1 \rangle$ and $\langle P_2 \rangle$, respectively. In our model the dipole is along the molecular symmetry axis. Therefore, the instantaneous value of P_2 is taken to be the largest eigenvalue of the ordering matrix, \mathbf{Q} , with elements defined by [15]

$$Q_{\alpha\beta} = \frac{1}{N} \sum_{i=1}^n \frac{1}{2} (3\mu_{\alpha}^i \mu_{\beta}^i - \delta_{\alpha\beta}), \quad (4)$$

where μ_{α}^i is the α component of the unit vector $\hat{\boldsymbol{\mu}}_i = (\mu)^{-1} \boldsymbol{\mu}_i$. The eigenvector corresponding to the largest eigenvalue is the instantaneous director $\hat{\mathbf{d}}$. Again, since the dipole moment is along the symmetry axis of the particle, we can define the instantaneous first-rank order parameter as [11,17]

$$P_1 = \frac{1}{N} \left| \sum_{i=1}^N \hat{\boldsymbol{\mu}}_i \cdot \hat{\mathbf{d}} \right|. \quad (5)$$

If the system considered is isotropic, both order parameters will have small, near-zero values (near zero rather than zero because we are considering systems of finite size). If the

system is ferroelectric, both order parameters will be non-zero. It is also possible to have systems which are ordered but antiferroelectric (e.g., polarized columns with equal numbers up and down). In this case $\langle P_1 \rangle$ will be near zero but $\langle P_2 \rangle$ will be nonzero.

In order to investigate the development of spatial structure, it is useful to calculate parallel (\parallel) and perpendicular (\perp) correlation functions, $g_{\parallel}(r_{\parallel})$ and $g_{\perp}(r_{\perp})$, respectively. If the instantaneous director is given by $\hat{\mathbf{d}}$, then \mathbf{r}_{\parallel} and \mathbf{r}_{\perp} are the vectors $\mathbf{r}_{\parallel} = (\mathbf{r} \cdot \hat{\mathbf{d}}) \hat{\mathbf{d}}$ and $\mathbf{r}_{\perp} = \mathbf{r} - \mathbf{r}_{\parallel}$. The correlation functions are defined as

$$g_{\parallel}(r_{\parallel}) = \frac{\langle n(r_{\parallel}, r_{\parallel} + \delta r_{\parallel}) \rangle}{\langle n_0(r_{\parallel}, r_{\parallel} + \delta r_{\parallel}) \rangle}, \quad (6)$$

$$g_{\perp}(r_{\perp}) = \frac{\langle n(r_{\perp}, r_{\perp} + \delta r_{\perp}) \rangle}{\langle n_0(r_{\perp}, r_{\perp} + \delta r_{\perp}) \rangle}. \quad (7)$$

In the parallel case, $\langle n \rangle$ is the average number of particles in a disk-shape shell perpendicular to $\hat{\mathbf{d}}$ at r_{\parallel} of width δr_{\parallel} and radius $[(L/2)^2 - r_{\parallel}^2]^{1/2}$, where L is the length of the simulation cell. In the perpendicular case, $\langle n \rangle$ is the average number of particles in a cylindrical shell about $\hat{\mathbf{d}}$ of radius r_{\perp} , width δr_{\perp} , and height $2[(L/2)^2 - r_{\perp}^2]^{1/2}$. In both cases $\langle n_0 \rangle$ is the average number of particles one would expect in the relevant shell calculated using the angle-averaged pair distribution function. In an isotropic or nematic fluid, both $g_{\parallel}(r_{\parallel})$ and $g_{\perp}(r_{\perp})$ will be one everywhere. Positional order parallel and/or perpendicular to the director will appear as peaks in these correlation functions. For example, columnar ordering results in a large peak in $g_{\perp}(r_{\perp})$ at $r_{\perp}=0$ and in peaks in $g_{\parallel}(r_{\parallel})$ at multiples of the particle height. Some structural and orientational information can also be obtained by calculating projections of the pair correlation function [11] and this was also done in the present simulations.

In addition to collecting structural information, we also checked for solidification by monitoring the mean square displacement $\langle |\mathbf{r}_i(t) - \mathbf{r}_i(0)|^2 \rangle$, where \mathbf{r}_i is the position vector of particle i at time t . Of course, in fluids this function will increase linearly in time at long times in accord with the Einstein relationship [15]; for solids it will rapidly become constant as t increases.

III. RESULTS AND DISCUSSION

It is usual to characterize hard oblate ellipsoids of revolution by specifying the breadth-to-height ratio b/a . For the present ‘‘soft’’ repulsive model we follow the same convention and set $b/a \equiv 2\sigma_1/2\sigma_3$ (see Fig. 1; note that $\sigma_1 = \sigma_2$ in the present case). The thermodynamic state of a system of dipolar oblate ellipsoids is then completely determined by fixing b/a , the reduced dipole moment $\mu^* = (\mu^2/\epsilon a^3)^{1/2}$, the reduced temperature $T^* = kT/\epsilon$ (k is the Boltzmann constant and T is the absolute temperature), and the reduced density $\rho^* = \rho ab^2$. In the present paper we examine systems of dipolar oblate particles with aspect ratios ranging from $1.2 \leq b/a \leq 3$ at various reduced temperatures and densities. A partial phase diagram is obtained and the phase behavior observed is rationalized by examining the local structure of the fluid.

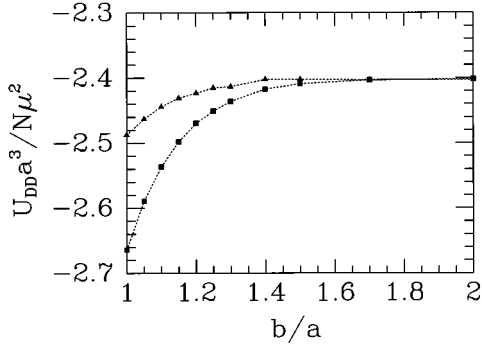


FIG. 2. The reduced dipolar energy per particle, $U_{DD}a^3/N\mu^2$, for different lattices of oblate dipolar particles. The triangles are for the antiferroelectric columnar lattice and the squares are for the ferroelectric tetragonal I lattice.

A. Dipolar lattice calculations

As a preliminary investigation, it is interesting to calculate the energy of two dipolar lattices chosen to be consistent with the observed *local* structure in ferroelectric nematic and antiferroelectric columnar phases. For dipolar spheres in the ferroelectric nematic phase the local structure resembles a tetragonal I crystal [11]. The tetragonal I structure is also the ground state of solids composed of dipolar spheres [18]. The antiferroelectric columnar phase has polarized columns arranged with hexagonal symmetry. The up or down arrangement of polarized columns is completely random and the net polarization of the system is zero [7,8]. Both lattices can be constructed by arranging columns of dipoles in an appropriate manner. In the antiferroelectric case the columns were first arranged on a hexagonal lattice and then equal numbers of columns were randomly oriented up or down. The dipole-dipole distance in the column was fixed at a and the reduced density at $\rho^* = 1$. Lattices corresponding to different values of b/a were then generated by expanding the system in directions perpendicular to the dipoles. The total dipole-dipole energy was calculated by employing the Ewald method.

The dimensionless dipole-dipole energy per particle, $U_{DD}a^3/N\mu^2$, obtained for both lattices is shown in Fig. 2. For reference, it is useful to note that for a single, isolated, infinite column of dipolar particles $U_{DD}a^3/N\mu^2 = -2.40$. From Fig. 2 we see that for spherical particles the ferroelectric lattice has the lowest energy. This is consistent with the observed local structure in ferroelectric fluids of dipolar spheres. As the aspect ratio is increased, the energies of both lattices approach the single infinite chain result and, in fact, for values of $b/a \geq 1.5$ the differences are insignificant. Thus the antiferroelectric behavior observed in fluids of dipolar cut spheres with $D/L = 10$ [7,8] can be explained simply in terms of entropy. The column-column interactions in the fluid are so weak that entropy ensures that equal numbers will be polarized in different directions. Finally, for small to intermediate aspect ratios (i.e., ≤ 1.5) the suggested ground state is a ferroelectric tetragonal I lattice. However, the behavior of the finite temperature fluids is not obvious from these lattice considerations and detailed simulations are required.

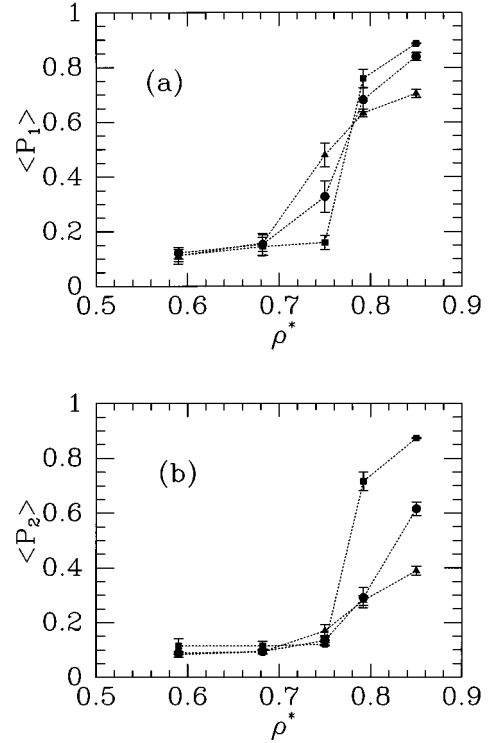


FIG. 3. The order parameters $\langle P_1 \rangle$ (a) and $\langle P_2 \rangle$ (b) as functions of reduced density at $T^* = 1.9$. The squares, circles, and triangles are for $b/a = 1.5, 1.3$, and 1.2 , respectively.

B. MD simulations

It is useful to begin by considering some MD results at $T^* = 1.9$ and $\mu^* = 3.0$. The average order parameters obtained for $b/a = 1.2, 1.3$, and 1.5 are shown as a function of density in Fig. 3. It must be emphasized that in the absence of dipolar interactions all three systems would be isotropic. Indeed, it is well known [3,4] that hard oblate ellipsoids do not have a liquid crystal phase for aspect ratios < 3 . Therefore any orientational order observed here arises mainly from the dipolar interactions. From Fig. 3, we see that all three systems undergo an orientational ordering transition near $\rho^* \approx 0.78$. Furthermore, the ordered phase is ferroelectric. Also, one notes that the transition becomes sharper and the ordering more pronounced as b/a is increased. This behavior is apparent both in $\langle P_1 \rangle$ [Fig. 3(a)] and $\langle P_2 \rangle$ [Fig. 3(b)]. Thus based on these particular simulations one might conclude that, at least for intermediate values, increasing b/a favors ferroelectric ordering. However, the situation is not so simple. If, for $b/a = 1.5$, the density scan is repeated at a lower temperature, one again finds orientational ordering as indicated by $\langle P_2 \rangle$ but no ferroelectric ordering is observed. For example, for $\rho^* = 0.792$, $\langle P_1 \rangle \approx 0.15$ at $T^* = 1.35$ compared with ~ 0.75 at $T^* = 1.9$.

This effect is clearly shown in Fig. 4 where the order parameters are plotted as a function of T^* for a system with $b/a = 1.45$ and $\rho^* = 0.792$. There is nothing special about these values of b/a and ρ^* and other systems exhibit similar behavior. From the plot we see that the system is polarized (i.e., $\langle P_1 \rangle$ is not zero) for a narrow temperature range around $T^* \approx 1.9$. Both above and below this temperature range $\langle P_1 \rangle$ is near zero. At higher temperatures $\langle P_2 \rangle$ is also ~ 0

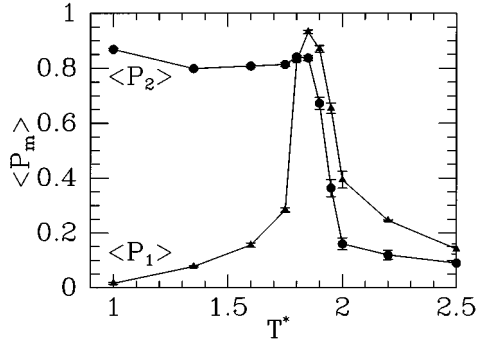


FIG. 4. The order parameters $\langle P_1 \rangle$ (triangles) and $\langle P_2 \rangle$ (circles) as functions of T^* at $b/a=1.45$ and $\rho^*=0.792$.

indicating that the system is simply isotropic. However, below $T^* \approx 1.9$, $\langle P_2 \rangle$ remains large despite the fact that $\langle P_1 \rangle$ is near zero. This indicates that at lower temperatures the system is orientationally ordered but unpolarized. This strongly suggests that at the lower temperatures strong columnar correlations develop resulting in an antiferroelectric columnar phase similar to that previously observed [7,8] for fluids of dipolar cut spheres with a much larger aspect ratio.

Evidence for this conclusion is provided in Fig. 5 where we show configurational “snapshots” for systems with $b/a=1.45$, $\rho^*=0.792$ at $T^*=1.35$, 1.9, and 2.5. We see that at $T^*=1.35$ [Fig. 5(a)] there is antiferroelectric columnar order. The columns are not very rigid and there is no obvious hexagonal order as one finds for larger aspect ratios. Nevertheless, the columns are polarized and approximately equal numbers are oriented in opposite directions such that there is no net polarization. As the temperature is increased to $T^*=1.9$ [Fig. 5(b)], the columnar structure weakens further and a ferroelectric phase is formed. At $T^*=2.5$ [Fig. 5(c)] the system is clearly isotropic and there is no orientational order of any kind.

The mean square displacements obtained for all three systems are shown as functions of the reduced time, t^* , in Fig. 6. We note that for all three phases $\langle |\mathbf{r}_i(t) - \mathbf{r}_i(0)|^2 \rangle$ increases continually with t^* indicating that all three are fluid. The diffusion becomes slower at lower temperatures (i.e., in the liquid crystal phases) but certainly remains finite.

It is interesting to consider $g_{\parallel}(r_{\parallel})$ and $g_{\perp}(r_{\perp})$ for the same systems. These functions are plotted in Fig. 7. We note that they exhibit no structural features at $T^*=2.5$, indicating that as expected the isotropic system has no long-range spatial correlations. At $T^*=1.9$ and 1.35, the peaks in $g_{\parallel}(r_{\parallel})$ and $g_{\perp}(r_{\perp})$ indicate that columnar correlations are present. The strong peak in $g_{\perp}(r_{\perp})$ [Fig. 7(a)] at $r_{\perp}^*=0$ arises from particles in the same column. The peaks at $r_{\perp}^* \sim 1.5$ and 3 result from near-neighbor and next-near-neighbor columns (recall that $b/a=1.45$). The sharp peaks in $g_{\parallel}(r_{\parallel})$ [Fig. 7(b)] at $r_{\parallel}^*=1, 2$, and 3 result from particles in the same column. The absence of peaks at ~ 1.5 and ~ 2.5 indicates that there is no significant interdigitation of the columns as one would expect with tetragonal-I-like correlations. As the temperature is decreased and the system passes from the ferroelectric phase ($T^*=1.9$) to the antiferroelectric phase ($T^*=1.35$) the columnar correlations become stronger but there is no sudden qualitative change. This suggests that as the ferro-

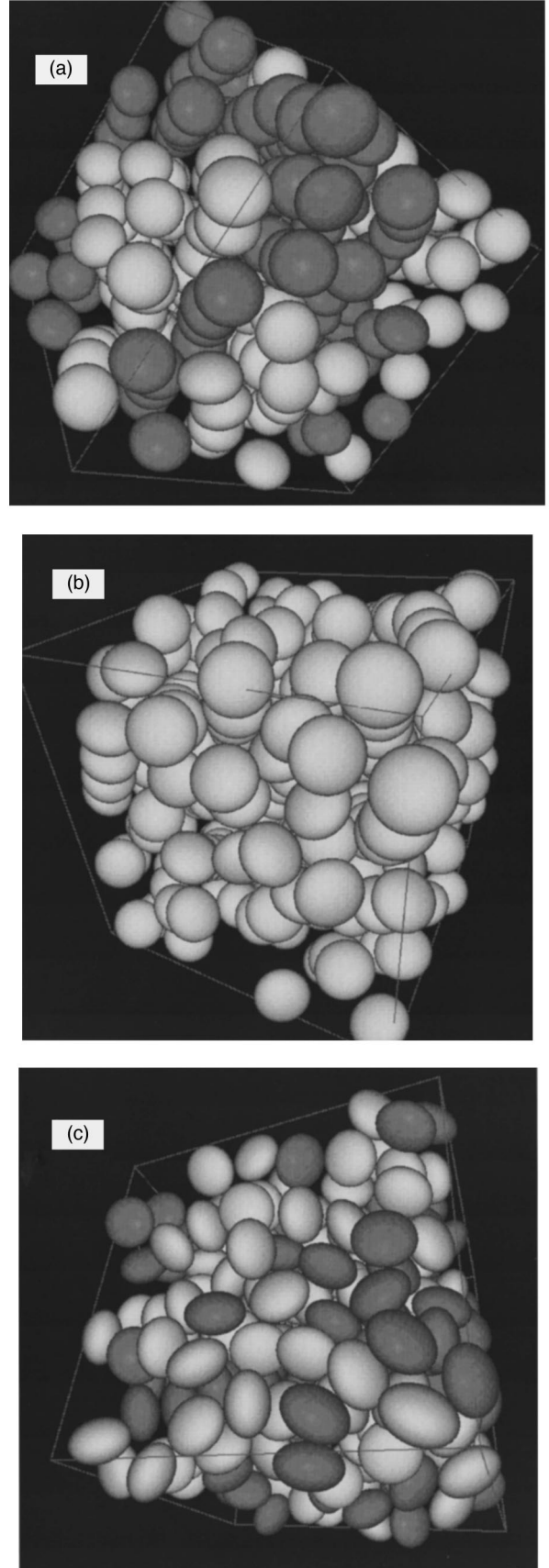


FIG. 5. Configurational snapshots of systems with $b/a=1.45$ and $\rho^*=0.792$ at $T^*=1.35$ (a), $T^*=1.9$ (b) and $T^*=2.5$ (c). The light and dark particles are oriented in opposite directions.

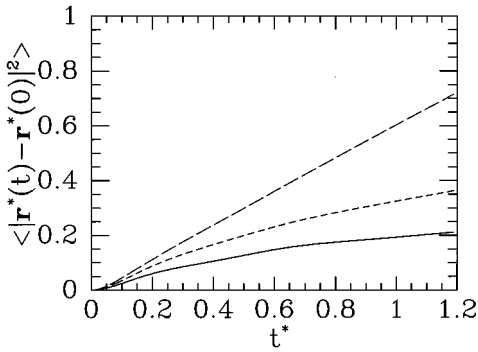


FIG. 6. Mean square displacements as functions of the reduced time t^* . The solid, dashed, and long-dashed lines are for $T^* = 1.35, 1.9,$ and $2.5,$ respectively.

electric phase is cooled the columnar correlations grow in length and strength until some critical condition is reached and the ferroelectric-antiferroelectric transition occurs. It is likely that this occurs when the columns are sufficiently “firm” and well enough defined to be regarded as separate entities which can be moved or inverted without significantly increasing the energy of the system. In other words, in the ferroelectric phase the fluid still behaves essentially as a system of independent particles; whereas, in the antiferroelectric phase it behaves more as a collection of columns.

It is also instructive to examine $g^{110}(r)$, which is the projection of the pair correlation function proportional to $\langle \hat{\mu}_1 \cdot \hat{\mu}_2 \rangle_r$, where the subscript r indicates that the average is evaluated at the separation r [11]. It is obvious that $g^{110}(r)$ is a direct measure of the tendency of the dipoles to align. In

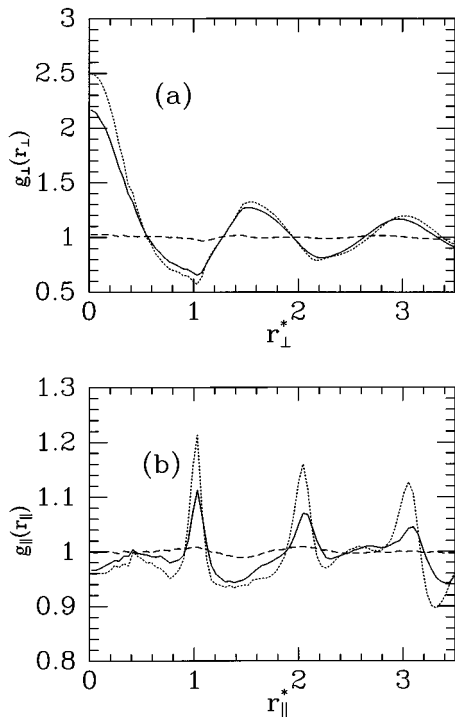


FIG. 7. The functions $g_{\perp}(r_{\perp})$ (a) and $g_{\parallel}(r_{\parallel})$ (b) for systems with $b/a = 1.45$ and $\rho^* = 0.792$. The solid, dotted, and dashed curves are for $T^* = 1.35, 1.9,$ and $2.5,$ respectively.

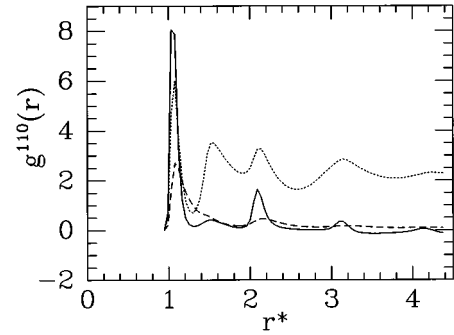


FIG. 8. The projection $g^{110}(r)$ for systems with $b/a = 1.45$ and $\rho^* = 0.792$. The solid, dotted, and dashed curves are for $T^* = 1.35, 1.9,$ and $2.5,$ respectively.

fact, in a ferroelectric phase without long-range spatial order, $g^{110}(r)$ becomes constant and proportional to $\langle P_1 \rangle$ as $r \rightarrow \infty$ [11]. In Fig. 8, $g^{110}(r)$ is plotted for the isotropic, ferroelectric, and antiferroelectric systems discussed above. It can be seen that in the isotropic phase, $g^{110}(r)$ has a relatively weak peak at $r^* = 1$ and decays rapidly to zero at larger separations as expected. In the ferroelectric phase, $g^{110}(r)$ is more strongly peaked at $r^* = 1$ and peaks also occur at $r^* \sim 1.5, 2,$ and 3 . The peak at ~ 1.5 is associated with particles in neighboring “columns.” The peak at ~ 2 is due to next-near neighbors in the same column and that at ~ 3 includes contributions from both the same and neighboring columns. Also in the ferroelectric phase, $g^{110}(r)$ approaches a nonzero constant at large r and we have verified that the value of this constant is consistent with the directly measured $\langle P_1 \rangle$. In the antiferroelectric phase the peaks at $r^* \approx 1$ and 2 are sharper indicating increased columnar order. Furthermore, the peak at $r^* \approx 1.5$ has essentially vanished indicating that it is equally likely to find the dipoles in neighboring columns in parallel or antiparallel orientations. This, together with the fact that $g^{110}(r)$ decays rapidly to zero, is strong evidence that in the low temperature phase columns polarized up or down occur more or less randomly and no domain structure exists.

It is also useful to consider the behavior of the average reduced energy, $\langle U^* \rangle / N \equiv \langle U \rangle / N\epsilon$, and heat capacity, $C_V^* / N \equiv C_V / Nk$, as functions of T^* and results for $b/a = 1.45$ and $\rho^* = 0.792$ are shown in Fig. 9. The heat

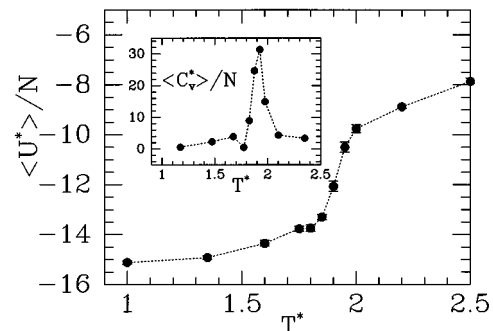


FIG. 9. The reduced configurational energy per particle as a function of T^* . The inset is the reduced excess heat capacity per particle.

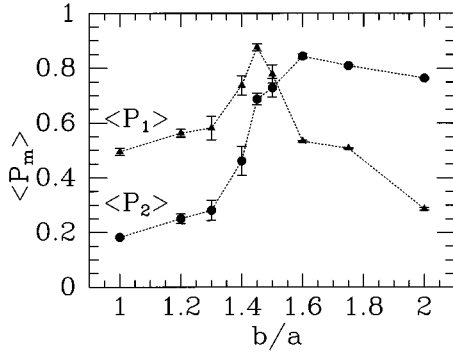


FIG. 10. The order parameters $\langle P_1 \rangle$ (triangles) and $\langle P_2 \rangle$ (circles) as functions of the aspect ratio at $T^* = 1.9$ and $\rho^* = 0.792$.

capacity (inset) was obtained by numerical differentiation of the average energy. The sudden drop in energy and the correspondingly sharp peak in heat capacity indicate the isotropic-ferroelectric transition at $T^* \approx 1.9$. There is also a small bump in the heat capacity at $T^* \approx 1.65$ which appears to be associated with the ferroelectric-antiferroelectric transition evident in the order parameter plot (Fig. 4).

The influence of particle anisotropy on ferroelectric order at fixed temperature and density is shown in Fig. 10. Here we have plotted the order parameters as a function of b/a at $T^* = 1.9$ and $\rho^* = 0.792$. We see that $\langle P_2 \rangle$ increases with increasing b/a , reaches a maximum at $b/a \approx 1.6$, and then decreases slightly for larger aspect ratios. The polarization increases with b/a for values ≤ 1.45 ; at $b/a = 1.45$ the system is strongly ferroelectric. For larger values of b/a , the polarization declines quite rapidly as columnar correlations grow and the antiferroelectric behavior discussed above becomes established.

C. Simple phase diagram

We have carried out a number of further simulations for different systems and the results are conveniently summarized in the partial ‘‘phase diagram’’ given in Fig. 11. Here we have plotted phase boundaries on a $(b/a, T^*)$ diagram and the stable phase in each region is indicated. The results

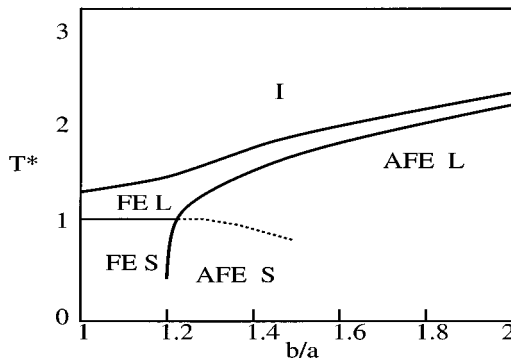


FIG. 11. An approximate phase diagram for dipolar oblate ellipsoids with $\mu^* = 3$ and $\rho^* = 0.792$. The phases indicated are isotropic (I), ferroelectric liquid (FE L), antiferroelectric liquid (AFE L), ferroelectric solid (FE S) and antiferroelectric solid (AFE S).

shown are for $\mu^* = 3$ and $\rho^* = 0.792$. This reduced density was chosen to emphasize the ferroelectric liquid region. For lower densities the isotropic phase would be stable at lower temperatures, while at higher densities the solid would occupy a larger region of the phase diagram. The phase boundary lines were obtained by examining the order parameters and the mean square displacement for selected systems. We emphasize that these lines were not obtained from rigorous thermodynamic calculations and are therefore approximate. Also, it must be noted that we do not know the ground state (zero temperature) crystal structures. The solids we refer to are those obtained simply by cooling the liquid until there was no significant diffusion. However, for larger aspect ratios where the particles do not freeze into a well defined lattice, it is not really possible to determine if a system has truly frozen or merely become a very viscous glass. For these systems the diffusion constant decreases essentially continuously as the system is cooled and does not provide a distinct transition temperature. To emphasize this uncertainty the estimated solid-liquid boundary in Fig. 11 is shown as a dashed line for $b/a > 1.2$. We make no estimate at all of the solidification temperature for $b/a > 1.5$.

In the near spherical regime (i.e., $b/a \leq 1.2$) we see behavior familiar from earlier work [11]. Upon cooling the isotropic phase a ferroelectric fluid is obtained which upon further cooling freezes to a ferroelectric solid. The structure of the solid is tetragonal I and the ferroelectric liquid crystal has local structure reminiscent of this.

At some aspect ratio above $b/a \approx 1.2$ two liquid crystal phases exist. When the isotropic system is cooled a ferroelectric phase is formed. In this phase the local structure is not tetragonal-I-like as in the spherical case, but there are short-range columnar correlations. Upon further cooling, the columnar order increases and what we may loosely call an antiferroelectric columnar fluid phase is formed. Thus the ferroelectric fluid is stable in a rather narrow temperature range between the isotropic and antiferroelectric fluids. As b/a is increased, the isotropic-ferroelectric and ferroelectric-antiferroelectric transition temperatures increase and move closer together. Thus, as b/a increases the temperature range of the ferroelectric phase decreases and eventually vanishes. For example, for $b/a = 2$ the ferroelectric-antiferroelectric transition is at $T^* \approx 2.3$ and the reduced temperature range of the ferroelectric is ~ 0.2 . For $b/a = 3$ we find no ferroelectric phase at all. These observations are not surprising. Particles with larger aspect ratios have a stronger tendency to form columns and eventually the system transforms directly from the isotropic to the antiferroelectric columnar phase without passing through a ferroelectric state.

IV. CONCLUSIONS

The purpose of this paper has been to explore the influence of particle shape upon the existence of ferroelectric liquid phases. It is shown that dipolar oblate particles exhibit rather interesting phase behavior. For aspect ratios $b/a \leq 1.2$ these systems form a single ferroelectric liquid crystal phase similar to that previously observed for dipolar spheres [11,12]. However, for larger aspect ratios two liquid crystal phases are found. Cooling of the isotropic phase yields a ferroelectric liquid with short-range columnar corre-

lations but no long-range spatial order. Upon further cooling the polarization vanishes and an antiferroelectric columnar liquid is formed. Thus the ferroelectric liquid exists over a temperature range between the isotropic and antiferroelectric columnar phases. As the aspect ratio is increased the temperature range for which the ferroelectric phase is stable becomes progressively narrower and eventually vanishes for values of $b/a \geq 3$. For aspect ratios ≥ 3 , the isotropic fluid transforms directly to the antiferroelectric columnar state without passing through the ferroelectric phase. This is consistent with earlier observations for dipolar cut spheres with large aspect ratios [7,8].

ACKNOWLEDGMENT

The financial support of the National Science and Engineering Research Council of Canada is gratefully acknowledged.

APPENDIX: REPULSIVE GAUSSIAN OVERLAP POTENTIAL

The Gaussian overlap model provides a continuous repulsive pair potential that is particularly suited for MD simulations of ellipsoidal particles.

Employing the notation of Ref. [14], the orientation and shape of a three dimensional Gaussian ellipsoid can be described by the tensor \mathbf{T} defined as

$$\mathbf{T} = \mathbf{R}' \mathbf{b} \mathbf{R}. \quad (\text{A1a})$$

Here \mathbf{b} is the tensor

$$\begin{pmatrix} 1/2\sigma_1^2 & 0 & 0 \\ 0 & 1/2\sigma_2^2 & 0 \\ 0 & 0 & 1/2\sigma_3^2 \end{pmatrix}, \quad (\text{A1b})$$

where σ_1 , σ_2 , and σ_3 are the principle radii of the ellipsoid cast in standard form (see Fig. 1). \mathbf{R} is a rotation matrix (its transpose is denoted \mathbf{R}') which expressed in quaternions has the form [15]

$$\begin{pmatrix} q_0^2 + q_1^2 - q_2^2 - q_3^2 & 2(q_1q_2 + q_0q_3) & 2(q_1q_3 - q_0q_2) \\ 2(q_1q_2 - q_0q_3) & q_0^2 - q_1^2 + q_2^2 - q_3^2 & 2(q_2q_3 + q_0q_1) \\ 2(q_1q_3 + q_0q_2) & 2(q_2q_3 - q_0q_1) & q_0^2 - q_1^2 - q_2^2 + q_3^2 \end{pmatrix}, \quad (\text{A1c})$$

where

$$q_0 = \cos \frac{1}{2} \theta \cos \frac{1}{2} (\phi + \psi), \quad (\text{A1d})$$

$$q_1 = \sin \frac{1}{2} \theta \cos \frac{1}{2} (\phi - \psi), \quad (\text{A1e})$$

$$q_2 = \sin \frac{1}{2} \theta \sin \frac{1}{2} (\phi - \psi), \quad (\text{A1f})$$

$$q_3 = \cos \frac{1}{2} \theta \sin \frac{1}{2} (\phi + \psi), \quad (\text{A1g})$$

and θ , ϕ , and ψ are the Euler angles [15].

The pair interaction is assumed to be proportional to the overlap integral of two Gaussian ellipsoids. For two identical ellipsoids at separation \mathbf{r} and with orientations defined by the quaternion sets \mathbf{q}_i and \mathbf{q}_j , the interaction energy $u(\mathbf{r}, \mathbf{q}_i, \mathbf{q}_j)$ is given by [14]

$$u(\mathbf{r}, \mathbf{q}_i, \mathbf{q}_j) = \frac{4\varepsilon \sqrt{|\mathbf{b}_i + \mathbf{b}_j|}}{\sqrt{|\mathbf{T}_i + \mathbf{T}_j|}} e^{s[1 + (\mathbf{B}\mathbf{B}/4A - \mathbf{C}) : \mathbf{r}\mathbf{r}]}. \quad (\text{A2})$$

If we define the tensor \mathbf{S} as

$$\mathbf{S} = \mathbf{T}_i + \mathbf{T}_j, \quad (\text{A3})$$

then

$$A = \frac{|\mathbf{T}_i + \mathbf{T}_j|}{S_{yy}S_{zz} - S_{yz}^2}, \quad (\text{A4})$$

and the components of the vector \mathbf{B} are

$$B_x = \frac{-2}{S_{yy}S_{zz} - S_{yz}^2} \begin{vmatrix} T_{j_{xx}} & T_{j_{xy}} & T_{j_{xz}} \\ S_{yx} & S_{yy} & S_{yz} \\ S_{zx} & S_{zy} & S_{zz} \end{vmatrix}, \quad (\text{A5a})$$

$$B_y = \frac{-2}{S_{yy}S_{zz} - S_{yz}^2} \begin{vmatrix} T_{j_{xy}} & T_{j_{yy}} & T_{j_{zy}} \\ S_{yx} & S_{yy} & S_{yz} \\ S_{zx} & S_{zy} & S_{zz} \end{vmatrix}, \quad (\text{A5b})$$

$$B_z = \frac{-2}{S_{yy}S_{zz} - S_{yz}^2} \begin{vmatrix} T_{j_{xz}} & T_{j_{yz}} & T_{j_{zz}} \\ S_{yx} & S_{yy} & S_{yz} \\ S_{zx} & S_{zy} & S_{zz} \end{vmatrix}. \quad (\text{A5c})$$

The elements of the symmetric tensor \mathbf{C} are

$$C_{xx} = T_{j_{xx}} - \frac{(S_{yz}T_{j_{xz}} - S_{zz}T_{j_{xy}})^2}{S_{zz}(S_{yy}S_{zz} - S_{yz}^2)} - \frac{T_{j_{xz}}^2}{S_{zz}}, \quad (\text{A6a})$$

$$C_{xy} = T_{j_{xy}} - \frac{(S_{yz}T_{j_{xz}} - S_{zz}T_{j_{xy}})(S_{yz}T_{j_{yz}} - S_{zz}T_{j_{yy}})}{S_{zz}(S_{yy}S_{zz} - S_{yz}^2)} - \frac{T_{j_{xz}}T_{j_{yz}}}{S_{zz}}, \quad (\text{A6d})$$

$$C_{yy} = T_{j_{yy}} - \frac{(S_{yz}T_{j_{yz}} - S_{zz}T_{j_{yy}})^2}{S_{zz}(S_{yy}S_{zz} - S_{yz}^2)} - \frac{T_{j_{yz}}^2}{S_{zz}}, \quad (\text{A6b})$$

$$C_{xz} = T_{j_{xz}} - \frac{(S_{yz}T_{j_{xz}} - S_{zz}T_{j_{xy}})(S_{yz}T_{j_{zz}} - S_{zz}T_{j_{zy}})}{S_{zz}(S_{yy}S_{zz} - S_{yz}^2)} - \frac{T_{j_{xz}}T_{j_{zz}}}{S_{zz}}, \quad (\text{A6e})$$

$$C_{zz} = T_{j_{zz}} - \frac{(S_{yz}T_{j_{zz}} - S_{zz}T_{j_{zy}})^2}{S_{zz}(S_{yy}S_{zz} - S_{yz}^2)} - \frac{T_{j_{zz}}^2}{S_{zz}}, \quad (\text{A6c})$$

$$C_{yz} = T_{j_{yz}} - \frac{(S_{yz}T_{j_{yz}} - S_{zz}T_{j_{yy}})(S_{yz}T_{j_{zz}} - S_{zz}T_{j_{zy}})}{S_{zz}(S_{yy}S_{zz} - S_{yz}^2)} - \frac{T_{j_{yz}}T_{j_{zz}}}{S_{zz}}. \quad (\text{A6f})$$

- [1] S. Chandrasekar, B.K. Sadashiva, and K.A. Sureshi, *Pramana* **9**, 471 (1977).
- [2] J.C. Dubois, *Ann. Phys. (N.Y.)* **3**, 131 (1978).
- [3] D. Frenkel, B.M. Mulder, and J.P. McTague, *Phys. Rev. Lett.* **52**, 287 (1984).
- [4] D. Frenkel and B.M. Mulder, *Mol. Phys.* **55**, 1171 (1985).
- [5] D. Frenkel, *Mol. Phys.* **60**, 1 (1987).
- [6] J.A.C. Veerman and D. Frenkel, *Phys. Rev. A* **45**, 5632 (1992).
- [7] J.J. Weis, D. Levesque, and G.J. Zarragoicoechea, *Phys. Rev. Lett.* **69**, 913 (1992).
- [8] G.J. Zarragoicoechea, D. Levesque, and J.J. Weis, *Mol. Phys.* **78**, 1475 (1993).
- [9] G.J. Zarragoicoechea, D. Levesque, and J.J. Weis, *Mol. Phys.* **75**, 989 (1992).
- [10] D. Levesque, J.J. Weis, and G.J. Zarragoicoechea, *Phys. Rev. E* **47**, 496 (1993).
- [11] D. Wei and G.N. Patey, *Phys. Rev. Lett.* **68**, 2043 (1992); *Phys. Rev. A* **46**, 7783 (1992).
- [12] J.J. Weis, D. Levesque, and G.J. Zarragoicoechea, *Phys. Rev. E* **48**, 3728 (1993).
- [13] B.J. Berne and P. Pechukas, *J. Chem. Phys.* **56**, 4213 (1972).
- [14] G. Ayton and G.N. Patey, *J. Chem. Phys.* **102**, No. 22, 9040 (1995).
- [15] M.P. Allen and D.J. Tildesely, *Computer Simulation of Liquids* (Clarendon, Oxford, 1989).
- [16] S.W. de Leeuw, J.W. Perram, and E.R. Smith, *Ann. Rev. Phys. Chem.* **37**, 245 (1986); *Proc. R. Soc. London, Ser. A* **373**, 27 (1980); **A388** (1983).
- [17] F. Biscarini, C. Zannoni, C. Chiccoli, and P. Pasini, *Mol. Phys.* **73**, 439 (1991).
- [18] R. Tao and J.M. Sun, *Phys. Rev. Lett.* **67**, 398 (1991).